The T^* Integral Parameter and its Applications to Dynamic Fracture Mechanics of Brittle Microcracking Solids

Y. TOI, T. NISHIOKA and S. N. ATLURI
Center for the Advancement of Computational Mechanics, Georgia Institute of Technology, Atlanta, Georgia 30332–0356, USA

Abstract

The continuum constitutive modeling for rate-dependent fracture of brittle microcracking solids, which was described in [1], is applied to the finite element analysis of rapidly propagating macrocracks under dynamic loading. The microcrack toughening effect is discussed, along with the influence on it of the crack propagation speed, through the observation of the behavior of the general crack-tip energy-release parameter, T^* integral [4, 5].

1 Introduction

The continuum constitutive modeling for rate-dependent fracture of brittle microcracking solids was presented in [1], which is an extension of the self-consistent modeling employed by Charalambides and McMeeking [9] to the rate-dependent problem including viscoplasticity. This modeling has been applied to the finite element analysis of static stationary and quasi-statically growing cracks under static loads in [2], in which the microcrack toughening effect has been discussed by observing the behavior of the general crack-tip energy-release parameter, the T^* integral. In the present paper, the same constitutive modeling is applied to the analysis of rapidly propagating cracks under dynamic loads, where the strain rate-effect plays a more important role than in the quasi-static analysis. In the present case also, the microcrack toughening effect is discussed, with the influence on it of the crack propagation speed, through the observation of the behavior of the crack-tip energy-release parameter, the T^* integral, for propagating cracks.

In Section 2 some remarks are made on the finite element calculations. In the following Section 3 a problem previously analyzed by Broberg [6], which deals with crack propagation with a constant speed in an infinite body under constant tension, is analyzed as an example of dynamic crack propagation problems. Note that Broberg [6] deals with linear elastic solids, whereas in the present work unmicrocracking as well as microcracking type nonlinear materials are treated. This problem is a standard problem in dynamic fracture mechanics, and an analytical solution is available to check the presently calculated solution for unmicrocracked materials. Emphasis is placed

on the difference of the solutions for unmicrocracking and microcracking materials. Especially the T^*-integral values are compared to discuss the microcrack toughening effect. Section 4 contains concluding remarks.

2 Finite Element Calculations

The constitutive modeling proposed in [1] has been implemented in the two-dimensional explicit elasto-viscoplastic finite element code contained in the finite element textbook [8], in which four-noded bilinear quadrilateral isoparametric elements are used with 2×2 Gaussian quadrature, and the explicit central difference time integration scheme is employed with lumped mass matrices.

In the present analysis, the crack-tip energy-release parameter for dynamically propagating cracks, T^*-integral [4] is calculated at each loading step by using the following domain integral expression [5], in order to discuss the microcrack toughening effect:

$$\begin{aligned} T^* &= \int_{\Gamma_\epsilon} [(W+T)n_1 - t_i(\partial u_i/\partial x_1)]\,\mathrm{d}\Gamma \\ &= -\int_{A-A_\epsilon} \{(W+T)(\partial S/\partial x_1) - \sigma_{ij}(\partial u_i/\partial x_1)(\partial S/\partial x_j)\}\mathrm{d}A \\ &\quad -\int_{A-A_\epsilon} \{\partial(W+T)/\partial x_1 - \sigma_{ij}(\partial \varepsilon_{ij}/\partial x_1) - \rho\ddot{u}_i(\partial u_i/\partial x_1)\}S\,\mathrm{d}A \end{aligned} \tag{1}$$

where

x_i : a system of Cartesian coordinates such that x_1 is along the crack axis, x_2 normal to the crack axis
Γ_ϵ : an arbitrary small loop surrounding the crack tip
A_ϵ : an area surrounded by Γ_ϵ
Γ_f : an arbitrary loop outside Γ_ϵ surrounding the crack tip
A : an area surrounded by Γ_f
t_i : the components in the x_i direction of the traction on the contour Γ_ϵ
u_i : the components in the x_i direction of displacements
n_1 : the component along the x_1 direction of a unit outward normal to the contour Γ_ϵ
W : the total stress-working density per unit volume defined by

$$W = \int_0^{\varepsilon_{ij}} \sigma_{ij}\,\mathrm{d}\varepsilon_{ij} \tag{2}$$

T : the kinetic energy per unit volume defined by

$$T = (1/2)\rho\dot{u}_i\dot{u}_i \tag{3}$$

S : an arbitrary continuous function such that

$$S = 1 \text{ on } \Gamma_\epsilon \quad \text{and} \quad S = 0 \text{ on } \Gamma_f \tag{4}$$

T^* integral has been chosen as a crack-tip parameter, since it is applicable to dynamic as well as static problems associated with any kind of material nonlinearities, and *unloading*. Details of the way to calculate this integral can be referred to in [2].

If the integrand on the right-hand side of Eq. (1) has a singularity of the order $(1/r)$ near the crack tip, for a Γ_ϵ of a circular geometry with radius ϵ, the integrand behaves as $(1/\epsilon)$ at Γ_ϵ where $\mathrm{d}\Gamma = \epsilon\,\mathrm{d}\theta$. Thus, T^* remains finite even in the limit as $\epsilon \to 0$. On the other hand, if the integrand has a weaker singularity than $(1/r)$, T^* tends to zero in the limit as $\epsilon \to 0$. However, in this latter case T^* has a finite value when evaluated on a finite-sized Γ_ϵ, say of a circular path of a small, but finite sized radius ϵ. In the present material model, with micro-cracking near the crack-tip, when micro-cracking saturates asymptotically close to the crack-tip, the material asymptotically near the crack-tip behaves linearly, with reduced elastic moduli. Thus, asymptotically close to the crack tip, the linear elastic type stress and strain singularities may be presumed to exist. Thus, the integrand in Eq. (1) is of the order $(1/r)$ and T^* has a finite value in the limit as $\epsilon \to 0$.

3 Analysis of Fast Dynamic Crack Propagation

3.1 Problem Description

A model problem of linear elastodynamic crack-propagation as defined by Broberg [6, 7] has been chosen as a numerical example for the present dynamic crack propagation analysis in a microcracking solid. This problem is illustrated in Fig. 1 which consists of an infinite body in equilibrium with a uniform axial tension, $\sigma_y = \sigma$, prior to crack extension. At $t = 0$ a crack begins to grow symmetrically, from an initial length of zero, at a constant rate $2c$ (each tip moves at speed c).

The analytical solution for the dynamic stress intensity factor given by Broberg [6] is dependent on the following two non-dimensional parameters:

$$c_L/c_S \qquad c/c_S$$

where c_L and c_S are respectively the longitudinal wave velocity and the shearing wave velocity, which are given by

$$c_L^2 = E(1-\nu)/\rho(1+\nu)(1-2\nu) \tag{5a}$$

$$c_S^2 = E/2\rho(1+\nu) \tag{5b}$$

In the present analysis the following values have been chosen:

$$\begin{aligned} c_L/c_S &= 2 \\ c/c_S &= 0.2,\ 0.4,\ \text{and } 0.6 \end{aligned}$$

The material constants assumed are as follows:

Young's modulus: $E = 0.123 \times 10^{12}$ (N/m^2)
Poisson's ratio: $\nu = 0.3333$
Critical stress for microcrack initiation: $\sigma_c = 0.2 \times 10^9$ (N/m^2)
Microcracking rate with stress: $\lambda = 0.74 \times 10^{-8}$ (m^2/N)
Saturated value of microcrack density: $\xi_s = 0.37$
Viscosity coefficient for microcrack density: $\eta = 0.1 \times 10^{-5}$ (1/sec)
Density of mass: $\rho = 3110$ (kg/m^3)

The crack propagation speed and the wave velocities are as follows:

$$\begin{aligned} c &= 0.077,\ 0.154 \text{ and } 0.231 \text{ (cm/}\mu\text{sec)} \\ c_L &= 0.770 \text{ (cm/}\mu\text{sec)} \\ c_S &= 0.385 \text{ (cm/}\mu\text{sec)} \end{aligned}$$

3.2 Finite Element Results

A sufficiently large rectangular-shaped area is assumed in order to avoid the effect of reflected wave during the analyzed time interval. Fig. 1 shows the mesh subdivision of the upper right quarter of the whole area, whose data is as follows:

Total number of elements = 1296
Total number of nodes = 1369
Total number of degrees of freedom = 2737 (initial value)

The crack propagation has been simulated by gradually releasing the nodal restraining force when the crack tip reaches that node. There are some elaborate techniques to deal with the dynamic crack propagation [4], however, the simplest technique has been used here, since the primary purpose of the present simulation is to gain a physical understanding of the phenomena including the microcrack toughening. The entire propagation length of 3.08 cm (20–element length) has been analyzed, using the following numbers of time steps and time increments: 400 steps with $\Delta t = 0.1\mu$sec for $c/c_S = 0.2$, 200 steps with $\Delta t = 0.1\mu$sec for $c/c_S = 0.4$, and 200 steps with $\Delta t = 0.0667\mu$sec for $c/c_S = 0.6$.

The analytical solution for the dynamic stress-intensity factor at the crack-tip, which propagates with a constant velocity c starting from a zero initial crack length is given by (Broberg [6]):

$$K_I = K(c)\hat{K}_I \tag{6}$$

where $K(c)$ is the so-called velocity factor, and $\hat{K}_I$ is the so-called static factor, which, in this case is: $\hat{K}_I = \sigma\sqrt{\pi a(t)}$ where $a(t)$ is the current half crack length, $a(t) = ct$ where c is the velocity of crack propagation. Broberg's [6] solution assumes that the solid is homogeneous, isotropic, and linearly elastic. In the present problem however, there is a zone of micro-crack-saturated material [which behaves linearly elastically] right near the propagating crack-tip; this is surrounded by a zone of *inelastic* material in which micro-cracking is still taking place, and the third zone of the solid consists once again of linear elastic isotropic material with constants E_u and ν_u corresponding to the virgin, unmicrocracked material. To understand the effect of microcracking on dynamic crack propagation, we compute the dynamic energy-release rate for a propagating crack, for the imposed K_I as in Eqs. (7) and (8), corresponding to two sets of elastic material constants: (i) E_u, ν_u of the uncracked virgin material; and (ii) $\bar{E}_s$ and $\bar{\nu}_s$ of the microcrack saturated material. The energy-release-rates for these cases are labeled here as T_u^* and T_s^* respectively. Using the well-known expressions for energy-release for propagating cracks, we write:

$$T_u^* = [A_I(c, E_u, \nu_u)K_I^2]/(2G_u) \tag{7}$$

$$T_s^* = [A_I(c, \bar{E}_s, \bar{\nu}_s)K_I^2]/(2\bar{G}_s) \tag{8}$$

where

$$\begin{aligned} A_I(c) &= \beta_1(1-\beta_2^2)/D(c) \\ D(c) &= 4\beta_1\beta_2 - (1+\beta_2^2)^2 \end{aligned} \tag{9}$$

$$\beta_1^2 = 1-(c/c_L)^2; \qquad \beta_2^2 = 1-(c/c_S)^2$$

Note that $A_I(c, \bar{E}_s, \bar{\nu}_s)$ in Eq. (8) has a negative value for the given material in the case of $c/c_S > 0.55$ when the crack speed c is larger than the Rayleigh wave speed. In order to avoid this situation, ν_s and c/c_L in Eq. (8) are assumed to keep their initial values as for the unmicrocracking solid in the present calculations. The imposed K_I corresponds with the given loading under these assumptions. Whichever definition of A_I in Eq. (8) is used for the case of $c/c_S < 0.55$, the following discussions are not influenced. The "exact" values of T_u^* and T_s^* as computed from Eqs. (7) and (8) are plotted as straight-lines in Fig. 2 for the value of $c/c_S = 0.4$. The numerically computed results, using the algorithm presented in Section 2 of this paper, for T_u^* of the uncracked material is also plotted as T_u^* (numerical) in this figure. That T_u^* (exact) and T_u^* (numerical) agree well indicates the numerical accuracy of the present finite element procedure of modeling dynamic crack propagation. The directly computed value T_m^* for the microcracking material, using the algorithm presented in Section 2, is also plotted in Fig. 2. That T_m^* is much smaller than T_s^* at all times indicates the toughening effect, caused by the material nonhomogeneity, especially the zone of *inelastic* microcracking material surrounding the microcrack-saturated material immediately near the crack-tip, in dynamic crack propagation in the presently considered class of materials.

Fig. 3 indicates the equivalent stress distribution ahead of the propagating crack-tip at $t = 15\mu$sec; for the two material models of (i) linear elastic isotropic solid without microcracking and (ii) with microcracking for the case of far-field $\sigma = 10^8$ N/m^2 and $c/c_S = 0.4$. considerable reduction in the magnitude of crack-tip stress intensity can be observed in Fig. 3.

In the following we discuss the quantitative effects of crack-speed, on the microcrack toughening.

For the applied stress of $\sigma = 10^8$ N/mm^2, and viscosity coefficient $\eta = 10^{-6}$/sec, the microcrack damage zone as "steady-state" conditions are obtained [at $t = 30\mu$sec, $\Delta a = 3.08$cm in the case $(c/c_S) = 0.2$; at $t = 15\mu$sec, $\Delta a = 3.08$cm in the case $(c/c_S) = 0.4$; and at $t = 10\mu$sec, $\Delta a = 3.08$cm in the case $(c/c_S) = 0.6$], are plotted in Fig. 4 for various values of crack-speed (c/c_S). In Fig. 4, each element in the finite element mesh near the crack tip is assigned a different symbol, depending on the level of microcracking. It is seen that the microcrack damage zone is the largest for the lowest crack-velocity, and decreases progressively as the crack-speed increases. Also, lower the crack-speed, the sooner in time is the level of microcrack saturation reached near the crack-tip. Also, the velocity factors $K(c)$ in Eq. (6), and $A_I(c)$ in Eqs. (7, 8) are valid for only linear elastic material behavior near the crack tip. For linear elasticity, $K(c)$ decreases with crack-speed, reducing the zero as $c = c_R$, the Raleigh wave speed. In the presence of a nonlinear inelastic material behavior near the crack-tip, the velocity factors for energy-release rate are unknown. In the microcracking solid, the nature and size of the nonlinear zone near the crack-tip depends on the crack-speed itself as seen from Fig. 4. However, if the "steady-state" values [at $\Delta a = 3.08$cm in Fig. 5] of (T_m^*/T_u^*) (normalized values of T_m^*) are compared, it is seen that this ratio decreases as (c/c_S) increases from 0.2 to 0.4, but the ratio T_m^*/T_u^* increases again as (c/c_S) increases from

0.4 to 0.6. For $(c/c_S) = 0.2$, an elastic zone develops near the crack-tip, at steady-state conditions, as seen from Fig. 4. Thus, the near-tip field in the case of $(c/c_S) = 0.2$, at steady state, can be seen to have an elastic singularity, and that the velocity factor in Eq. (6) can also be estimated by the near-tip elastic properties. Thus, one may estimate the energy-release-rate T_m^*, from the equation:

$$T_m^* = [A_I(c, \bar{E}_s, \bar{\nu}_s) K_{\text{tip}}^2]/(2\bar{G}_s) \tag{10}$$

where

$$A_I = \beta_1[1 - \beta_2^2]/[4\beta_1\beta_2 - 1 + \beta_2^2] \tag{11a}$$

$$\beta_1^2 = 1 - (c/c_L)^2; \qquad \beta_2^2 = 1 - (c/c_S)^2 \tag{11b}$$

$$c_L^2 = [\bar{E}_s(1 - \bar{\nu}_s)]/\rho(1 + \bar{\nu}_s)(1 - 2\bar{\nu}_s) \tag{11c}$$

$$c_S^2 = \bar{E}_s/[2\rho(1 + \bar{\nu}_s)] \tag{11d}$$

It can easily be calculated for the present case of material properties,

$$\frac{A_I(c, \bar{E}_s, \bar{\nu}_s)}{A_I(c, E_u, \nu_u)} = 1.41 \qquad \text{for } c = 0.2c_S \tag{11e}$$

$$G_u/\bar{G}_s = 2.44$$

By curve fitting the asymptotic stress field in the unmicrocracked case, and in the microcracked case, at $t = 37\mu$sec, for $(c/c_S) = 0.2$, it is seen that $(K_{\text{tip}}/K_I) \approx 0.5$. Thus, evaluating T_m^* from Eq. (11), and T_u^* from Eq. (9), we compute

$$\frac{T_m^*}{T_u^*} \approx 0.86 \tag{11}$$

This estimation of $T_m^* \approx 0.86 T_u^*$ agrees very well with the directly computed result *at steady-state*, as shown in Fig. 5.

4 Concluding Remarks

The rapidly propagating cracks, under dynamic loading, in brittle microcracking solids have been analyzed by the finite element method. The obtained results can be summarized as follows:

(1) The crack tip integral T^* should be used as the parameter describing the severity of the crack tip in the discussion of the microcrack toughening effect, because it is applicable to dynamic as well as quasi-static problems including any type of materially nonlinear behaviors, and *unloading*.

(2) The microcrack toughening effect exists in dynamic fracture of brittle microcracking solids. However, the magnitude of this toughening depends in a rather complicated way on the applied far-field stress, veclocity of crack-propagation, and the viscosity coefficients in the microcracking evolution equation [3].

(3) The "velocity factor" in the energy-release-rate expression depends simply on the material properties near the propagating crack-tip. When microcracking reaches a saturation near the propagating crack-tip, under specific conditions of applied stress, velocity of crack-propagation, and η, the velocity factor is as if for a linear elastic material with the reduced moduli corresponding to the microcrack-saturated material.

Acknowledgements

The support of the work by ONR, and the encouragement of Dr. Y. Rajapakse are gratefully acknowledged. It is a pleasure to thank Ms. Deanna Winkler for her assistance in preparing this paper.

References

1. Y. Toi and S.N. Atluri: Finite Element Analysis of Static and Dynamic Fracture of Brittle Microcracking Solids (Part 1: Formulation and Simple Numerical Examples), to be published.

2. Y. Toi and S.N. Atluri: Finite Element Analysis of Static and Dynamic Fracture of Brittle Microcracking Solids (Part 2: Static and Growing Macro-Cracks Under Static Loading), to be published.

3. Y. Toi and S.N. Atluri: Finite Element Analysis of Static and Dynamic Fracture of Brittle Microcracking Solids (Part 3: Stationary and Rapidly-Propagating Cracks Under Dynamic Loading), to be published.

4. S.N. Atluri (Editor): Computational Methods in the Mechanics of Fracture, Vol. 2 of Computational Methods in Mechanics, First Series of Handbooks on Mechanics and Mathematical Methods, North-Holland, (1986).

5. G.P. Nikishkov and S.N. Atluri: An Equivalent Domain Integral Method for Computing Crack-Tip Integral Parameter in Non-Elastic, Thermo-Mechanical Fracture, Engineering Fracture Mechanics, Vol. 26, No. 6, (1987), 851-867.

6. K.B. Broberg: The Propagation of a Brittle Crack, Arkiv fur Fysik, 18, (1960), 159-192.

7. J.A. Aberson, J.M. Anderson, and W.W. King: Dynamic Analysis of Cracked Structures Using Singularity Finite Elements, Chapter 5 in Elastodynamic Crack Problems (edited by G.C. Shih), Mechanics of Fracture 4, Noordhoff International Publishing, (1977), 249-294.

8. D.R.J. Owen and E. Hinton: Finite Elements in Plasticity; Theory and Practice, Pineridge Press Ltd., (1980).

9. P.G. Charalambides and R.M. McMeeking: Finite Element Method of Crack Propagation in a Brittle Microcracking Solid, Mechanics of Materials, 6, (1987), 71-87.

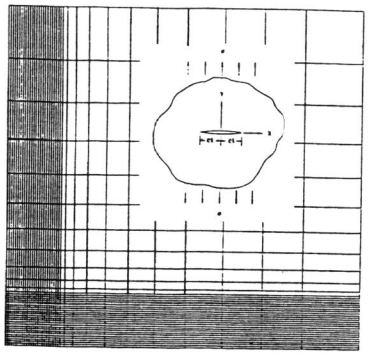

Fig. 1 Finite element mesh subdivision (one quarter)

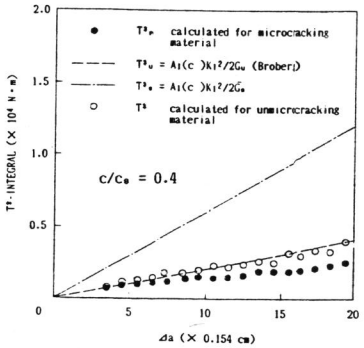

Fig. 2 Time histories of T^*-integral for the propagating crack (σ = 0.10 × 10^9 (N/m^2), η = 0.1 × 10^{-5} (1/sec))

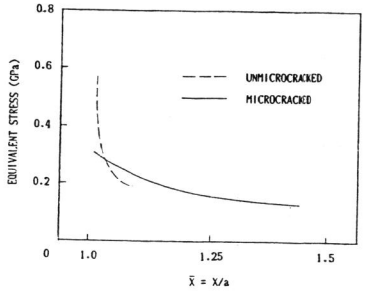

Fig. 3 Equivalent stress distribution at t = 15μsec (c/c_e = 0.4, σ = 0.10 × 10^9 (N/m^2), η = 0.1 × 10^{-5} (1/sec))

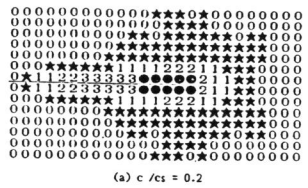

(a) c /cs = 0.2

(b) c /cs = 0.4

(c) c /cs = 0.6

★: 0.0 < ξ < 0.1 (initiation) 1: 0.1 ≦ ξ < 0.2
2: 0.2 ≦ ξ < 0.3 3: 0.3 ≦ ξ < 0.37
©: ξ = 0.37 (saturation at one Gaussian point)
●: ξ = 0.37 (saturation at more than one Gaussian points)

Fig. 4 Microcracked zones for different crack velocities (σ = 0.10 × 10^9 (N/m^2), η = 0.1 × 10^{-5} (1/sec))

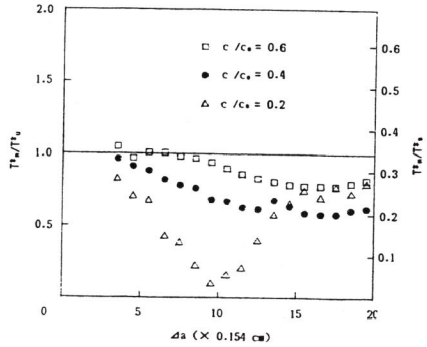

Fig. 5 Time histories of T^*-integral for different crack velocities (σ = 0.10 × 10^9 (N/m^2), η = 0.1 × 10^{-5} (1/sec))